Eccentrically loaded brickwork: Theoretical and experimental results

A. Brencich *, C. Corradi, L. Gambarotta

DICAT - Department of Civil, Environmental and Architectural Engineering, University of Genoa, Italy

ARTICLE INFO

ABSTRACT

The assessment procedures for masonry arches and columns usually assume homogeneous constitutive models for which strength and stiffness parameters are described in terms of a uni-axial constitutive law. The limits of such an approach are seldom discussed and related to the brickwork inhomogeneity, i.e. to the brick size and to the masonry bond. In this paper, a first theoretical and experimental approach to concentric and eccentric loading of solid clay brickwork are developed and discussed, investigating the failure modes and the compressive strength of masonry and their dependence on the strength, on the geometry of the constituents and on the loading conditions. A mechanical model for the load carrying capacity of eccentrically compressed brickwork prisms, based on the Static Theorem of Limit Analysis, is proposed allowing: (i) the compressive strength to be related to the size of bricks and mortar joints, showing that edge effects at the free edges do not significantly affect the global behaviour of the material; (ii) the limit domains in the axial force-bending moment space to be derived. Moreover, a series of brickwork prisms have been tested with different load eccentricities; the comparison with the theoretical approach provides upper and lower bounds to the load carrying capacity of the material and shows that: (i) brickwork exhibits limited inelastic strains that need to be taken into account to explain the experimental data; (ii) plastic models for masonry overestimate the actual load carrying capacity. On the basis of these results, one-dimensional homogenized constitutive models, suitable for applications, are formulated and their effectiveness supported by the experimental results.

© 2008 Elsevier Ltd. All rights reserved.

1. Introduction

Masonry structures are usually designed to sustain mainly axial forces; unfortunately, due to the variety of loading conditions, eccentricity of the axial thrust is unavoidable. The assessment procedures for eccentrically loaded masonry elements, i.e. arches, pillars and veneer walls are usually simplified and refer to homogeneous beam models for which the stress–strain response of the material is described in terms of uni-axial constitutive laws with reduced number of parameters. The reliability of such an approach, directly derived from the r.c. design procedures, is seldom discussed; instead, it should be carefully addressed since masonry is a heterogeneous material for which the size of the units (bricks) is of the same order of magnitude as the relevant structural size (cross section).

The homogeneous beam approach implicitly neglects the actual stress state in the material and the effect of the internal structure of masonry, considering average quantities only, i.e. axial thrust, shear force and bending moment. According to the classical beam theory, a compressive strength for masonry is also defined; it has to be considered as a parameter of the model rather than a local

limit stress since the beam approach is in itself global and does not consider any local phenomenon.

At the scale of the brick units, instead, the stress and strain states are inhomogeneous and may exhibit stress concentrations; consequently, the constitutive models need to be related to the mechanical properties of the constituents (bricks and mortar), to the geometry of the brickwork bond, to the ratio of the component size (brick size and mortar joint thickness) to the overall size of the structural element (essentially the size of the cross section) and to the load eccentricity. To this aim, while an overall elastic modulus may be defined on the basis of appropriate homogenization techniques [1], the load carrying capacity of masonry should be estimated taking into account the stress localizations in the constituents and the edge effects, i.e. representing masonry as a two-phase composite material [2].

The first proposed models [3–6, among the others] refer to brick walls subjected to uniform compressive stresses and represented as an unbounded layered medium. Interlayer compatibility of elastic strains results in a tensile-compressive stress field in the brick governing the collapse of the brick layer and, as a consequence, of the masonry wall. Despite the clear interpretation of compressive failure provided by this approach, the assumption of layered material ignores the mortar head joints and the free boundaries [7] while the assumption of uniform stress neglects the effect of the stress gradient, due to eccentric loading, on the load carrying capacity of brickwork. Improvements to these models

---

* Corresponding author. Tel.: +39 0103532512; fax: +39 0103532534.
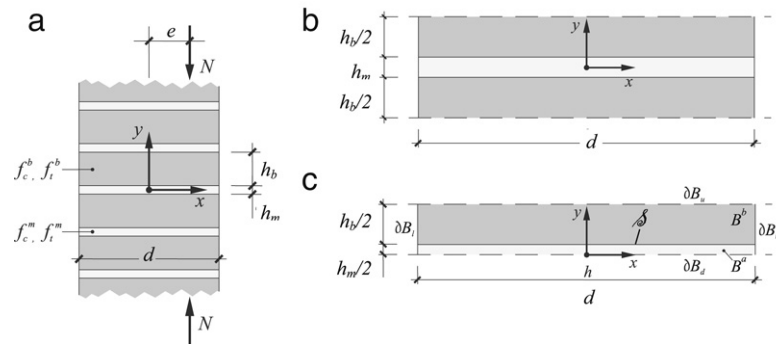*E-mail address:* brencich@dicat.unige.it (A. Brencich).

Fig. 1. (a) Eccentrically compressed column; (b) unit cell; (c) representative volume element.

have been developed for compressed brick masonry walls in [8, 9] based on an application of the Static Theorem of the Limit Analysis to a prescribed local stress field in the representative volume element. Nevertheless, since the analysis was devoted to large walls, these models ignore boundary effects and/or eccentric loading.

In the last thirty years, experimental research was carried out on this issue [10–19] but some aspects of the response of eccentrically loaded masonry seem to be not yet fully understood. Bearing in mind the homogeneous beam approach, assuming on the cross section a linear distribution of strains (Navier–Bernoulli), a vanishing tensile strength and an elastic brittle response in compression, recalling the pioneering work by Castigliano [20], some authors report an increase of the masonry compressive strength, up to twice the value measured for concentric loading (and uniform stress state), as the load eccentricity is raised [10–16]: this would imply that the compressive strength depends not only on the material properties but also on the eccentricity of the load. On the basis of other experimental data, taking into account a non linear compressive response [17,21,22] other authors [17–19] argue that this strength increase is only apparent and is due to the inelastic response of masonry as it approaches its ultimate strength. This controversial approach is reflected also in masonry codes: the UIC code allows a strength increase for eccentric loading [23], with an increase up to 60% of the concentric value, while Euro Code 6 [24] assumes the compressive strength as independent on the loading conditions.

In this paper, a first contribution to the compressive strength of solid clay brickwork is provided from both a theoretical and experimental approach. An inhomogeneous stacked perfectly-plastic periodic material is assumed for brickwork, for which proper stress functions, in the brick and in the mortar, allow statically admissible stress fields to be defined; the mathematical structure of the stress functions allows the free edges conditions to be represented. On the basis of the Static Theorem of Limit Analysis, assuming a Mohr–Coulomb type limit condition for both clay and mortar, the load carrying capacity of brickwork is addressed by means of the limit domain in the axial thrust-bending moment space, where the strength properties of masonry are better and unambiguously represented. The effect of the perturbation of the stress field, due either to the free edges and to the elastic mismatch between the bricks and mortar, on the collapse mechanism and on the ultimate load is taken into account.

Concentrically and eccentrically loaded prisms have also been tested for a direct comparison between theoretical previsions and experimental outcomes. The assumption of perfectly-plastic periodic material, unavoidable in the frame of a Limit Analysis approach, is showed to overestimate the actual load carrying capacity of solid clay brickwork.

Simplified homogeneous beam-like models are also discussed and their reliability for engineering applications in the assessment of masonry arch-type structures is analysed. Since these models are characterized by low levels of detail because of their phenomenological origin, they provide simple formulas for the limit strength domains in the axial force N, bending moment M plane that are compared to the experimental results, showing that the actual response of brickwork is in-between that of a perfectly brittle material and of a perfectly plastic one.

The theoretical approach discussed in this paper relies on the Static Theorem of Limit Analysis; therefore, it provides lower bounds to the load carrying capacity of solid clay brickwork. Since Limit Analysis is based on the assumption of a perfect plastic material response and plain strain conditions, and since bricks and mortar are quasi-fragile, the presented theoretical approach provides overestimations of the load carrying capacity if compared to the experimental values. The comparison of the theoretical results with a wide set of experimental results allows detailed discussion including a simple and conservative approach to the assessment of eccentrically loaded masonry structures.

2. Limit analysis of eccentrically compressed prisms

Let us consider the stack bond masonry prism of Fig. 1a consisting of clay brick units (width: d, height: h_b) and mortar joints (height: h_m). The prism is eccentrically compressed with axial force N ($N < 0$ in compression), bending moment M and eccentricity $e = M/N$; the weight of the prism is neglected.

The finite width d is the relevant aspect of this model in comparison to the unbounded layered medium of the Hilsdorf model [3] and other similar approaches. While in the latter case the stress state at the limit state (collapse) is homogeneous in each of the two phases (brick and mortar), the finite width assumption requires edge effects to be considered, thus leading to an inhomogeneous stress state in both the phases. In particular, the stress field in bricks and mortar can be assumed as the superposition of an homogeneous stress field (as for the unbounded model) and a perturbed stress field due to the free edges boundary conditions.

For Limit Analysis to be applicable, a perfect plastic response of the materials needs to be postulated, which is quite a relevant assumption for quasi-brittle materials such as clay brickwork and mortar. Besides, for the Static Theorem to be applied, statically admissible stress fields need to be considered taking into account the periodic arrangement of the brick units and the mortar layers through a representative unit cell, Fig. 1b. Because of the symmetry at mid-height of both the brick units and the mortar layer, a reduced domain can be considered, Fig. 1c, where B^b and B^m represent the brick unit and the mortar layer, respectively. The brick-mortar interface $\mathscr{S}$ is given a unilateral frictional contact constitutive model with associated Coulomb frictional sliding-dilatancy. The assumption of vanishing tensile strength of the interface allows to include the no-tension response into Limit

Analysis since in the true collapse mechanism no internal dissipation is considered in the interface opening mechanisms [25–28].

The residual source of approximation is the compressive perfectly plastic response for materials that are, in fact, quasi-fragile. Detailed discussion on this issue is carried out when comparing the theoretical outcomes to the experimental results.

For both the brick units and the mortar layers the Mohr–Coulomb criterion is the assumed limit condition, thus taking into account the multiaxial stress state in the brick unit and in the mortar layer. Plane strain conditions are considered referring to a slice of unitary depth; this constitutive assumption provides an overestimation of the load carrying capacity since it represents the limit conditions at the centre of a thick prism [2].

Equilibrated stress fields $\boldsymbol{\sigma} = \{\sigma_{xx} \quad \sigma_{yy} \quad \sigma_{xy}\}^{\mathrm{T}}$ are obtained by defining two Airy stress functions [29], Φ^m, Φ^b, referred to the mortar and the brick domains, respectively; the stress field takes the usual form $\boldsymbol{\sigma} = \{\Phi_{,yy} \quad \Phi_{,xx} \quad -\Phi_{,xy}\}^{\mathrm{T}}$, where the subscripts represent the derivatives.

The internal forces on each section are given as:

$$N = \int_{-\frac{d}{2}}^{\frac{d}{2}} \Phi^{\alpha}_{,xx} \mathrm{d}x, \quad \alpha = b, m, \tag{1a}$$

$$M = Ne = \int_{-\frac{d}{2}}^{\frac{d}{2}} \Phi^{\alpha}_{,xx} x \mathrm{d}x, \quad \alpha = b, m, \tag{1b}$$

$$V = \int_{-\frac{d}{2}}^{\frac{d}{2}} \Phi^{\alpha}_{,xy} \mathrm{d}x = 0, \quad \alpha = b, m, \tag{1c}$$

where V is the shearing force. The symmetry of the normal stress components σ_{xx} and σ_{yy} and the antisimmetry of the shear stresses σ_{xy} in the brick and mortar domains with respect to the boundaries ∂B_u and ∂B_d, respectively, imply the boundary conditions:

$$\Phi^b_{,xxy} = \Phi^b_{,yyy} = 0, \qquad \Phi^b_{,xy} = 0 \quad \text{on } \partial B_u, \tag{2a}$$

$$\Phi^m_{,xxy} = \Phi^m_{,yyy} = 0, \qquad \Phi^m_{,xy} = 0 \quad \text{on } \partial B_d. \tag{2b}$$

Moreover, the condition of free lateral edges $\sigma_{xx} = \sigma_{xy} = 0$ on ∂B_r and ∂B_l, together with the local equilibrium equation $\sigma_{xx,x} + \sigma_{xy,y} = 0$ lead to:

$$\Phi^{\alpha}_{,yy} = \Phi^{\alpha}_{,xy} = \Phi^{\alpha}_{,xyy} = 0 \quad \text{on } \partial B_r \text{ and } \partial B_l, \ \alpha = b, m. \tag{3}$$

At the interface $\mathcal{S}$ the stress functions have to guarantee the continuity of the stress field, i.e. the vanishing of stress jump $[\![\sigma_{yy}]\!] = 0$, $[\![\sigma_{xy}]\!] = 0$:

$$\Phi^m_{,yy} = \Phi^b_{,yy}, \qquad \Phi^m_{,xy} = \Phi^b_{,xy} \quad \text{on } \mathcal{S}. \tag{4}$$

The stress fields may be represented assuming the stress function in the form:

$$\Phi^{\alpha}(x, y) = z_0 \left[f_0^e(x) + \rho f_0^o(x)\right] + \sum_{r=1}^{R} \sum_{s=1}^{S} z_{rs}^{\alpha} f_r(x) g_s^{\alpha}(y),$$

$$\alpha = b, m \tag{5}$$

requiring a set of $2 + R + S$ functions, coefficients z_0, ρ, and a set of $2(1 + RS)$ coefficients z_{rs}^{α} to be selected. The form (5) for the stress functions makes use of the standard choice of separating the variables x and y and satisfies the static boundary conditions on the cross section (1c), on the upper and lower surfaces (2) and on the left and right borders (3). Besides, conditions (3) and (4) ask:

(i) functions $f_0^e(x)$ and $g_s^{\alpha}(y)$ ($\alpha = b, m, s = 1, S$) to be even;
(ii) function $f_0^o(x)$ to be odd;
(iii)

$$f_r = (f_r)' = 0 \quad \text{on } \partial B_r \text{ and } \partial B_l, \tag{6a}$$

(iv)

$$\left(g_s^m\right)' = \left(g_s^m\right)''' = 0 \quad \text{on } \partial B_d, \tag{6b}$$

(v)

$$\left(g_s^b\right)' = \left(g_s^b\right)''' = 0 \quad \text{on } \partial B_u, \tag{6c}$$

where superscripts $'$ and $'''$ stand for the first and third derivatives.

Moreover, the stress continuity condition (4) at the interface $\mathcal{S}$ implies further restrictions involving the coefficients in the form of homogeneous linear equations:

$$\sum_{s=1}^{S} z_{rs}^m g_s^m \big|_{\mathcal{S}} = \sum_{s=1}^{S} z_{rs}^b g_s^b \big|_{\mathcal{S}}; \qquad \sum_{s=1}^{S} z_{rs}^m \left(g_s^m\right)' \big|_{\mathcal{S}} = \sum_{s=1}^{S} z_{rs}^b \left(g_s^b\right)' \big|_{\mathcal{S}}$$

$$\text{for } r = 1, \ldots, R. \tag{7}$$

It follows that the coefficients z_0 and ρ are obtained from Eqs. (1a) and (1b):

$$z_0 = N \Big/ \int_{-\frac{d}{2}}^{\frac{d}{2}} \left(f_0^e(x)\right)'' \mathrm{d}x,$$

$$\rho = \left(\int_{-\frac{d}{2}}^{\frac{d}{2}} \left(f_0^e(x)\right)'' \mathrm{d}x \Big/ \int_{-\frac{d}{2}}^{\frac{d}{2}} \left(f_0^o(x)\right)'' x \mathrm{d}x\right) e, \tag{8}$$

and depend on the axial force N and eccentricity e, respectively. The stress function at a point in the domain $B^m \cup B^b$ can be expressed in the linear form $\Phi(x, y) = \boldsymbol{\Phi}^{\mathrm{T}} \mathbf{z}$, where $\boldsymbol{\Phi} = \{\Phi_0 \ \Phi_{11}^m \ldots \Phi_{RS}^m \ \Phi_{11}^b \ldots \Phi_{RS}^b\}^{\mathrm{T}}$ is the vector collecting the set of assumed stress functions $\Phi_0 = f_0^e(x) + \rho f_0^o(x)$, $\Phi_{rs}^{\alpha} = f_r(x) g_s^{\alpha}(y)$ and $\mathbf{z} = \{z_0 \ z_{11}^m \ldots z_{RS}^m \ z_{11}^b \ldots z_{RS}^b\}^{\mathrm{T}}$ is the vector collecting the $1 + 2RS$ unknown coefficients, where $g_s^m(y) = 0$ in B^b and $g_s^b(y) = 0$ in B^m. The stress field in the brick and mortar domains can be represented in the compact form $\boldsymbol{\sigma} = \mathbf{L}\boldsymbol{\Phi}^{\mathrm{T}}\mathbf{z}$, being $\mathbf{L} = \left\{\dfrac{\partial^2}{\partial y^2} \quad \dfrac{\partial^2}{\partial x^2} \quad -\dfrac{\partial^2}{\partial x \partial y}\right\}^{\mathrm{T}}$ a differential operator, together with the linear homogeneous equations from conditions (7) written in the form $\mathbf{S}\mathbf{z} = \mathbf{0}$, $\mathbf{S}$ being a proper matrix.

To obtain a Linear Programming (LP) formulation the Mohr–Coulomb limit domain for plane strain condition is approximated according to Sloan [30] with a inner polytope having K planes in the space of the stress components so that the unknown vector $\mathbf{z}$ is subjected to the following inequalities:

$$\mathbf{m}_k^{\alpha \mathrm{T}} \mathbf{L}\boldsymbol{\Phi}^{\mathrm{T}}\mathbf{z} \leq D^{\alpha}, \quad k = 1, \ldots, K, \alpha = m, b, \tag{9}$$

$$\mathbf{m}_k^{\alpha} = \{A_k^{\alpha} \quad B_k^{\alpha} \quad C_k^{\alpha}\}^{\mathrm{T}}.$$

Being:

$$A_k^{\alpha} = \sin \varphi^{\alpha} \cos (\pi/K) + \cos (2\pi k/K),$$

$$B_k^{\alpha} = \sin \varphi^{\alpha} \cos (\pi/K) - \cos (2\pi k/K),$$

$$C_k = 2 \sin (2\pi k/K),$$

$$D^{\alpha} = 2c \cos \varphi^{\alpha} \cos (2\pi k/K),$$

φ^{α} and c^{α} the friction angle and cohesion of the phase α, respectively (depending on the compressive f_c^m, f_c^b, and the tensile f_t^m, f_t^b, strength of mortar and brick).

The unilateral frictional contact conditions $\sigma_{yy} \leq 0$ and $|\sigma_{xy}| + \mu\sigma_{yy} \leq 0$ assumed at the interface $\mathcal{S}$ imply the linear inequalities:

$$\mathbf{Q}\boldsymbol{\sigma} = \mathbf{Q}_S \mathbf{L}\boldsymbol{\Phi}^{\mathrm{T}}\mathbf{z} \leq \mathbf{0}, \tag{10}$$

involving the unknown vector $\mathbf{z}$ of the unknown variables and matrix $\mathbf{Q}_S$ that depends on the friction coefficient μ.

The plastic admissibility conditions (9) and (10) are approximately imposed at a finite number ($2P \times Q$) of points defined on a
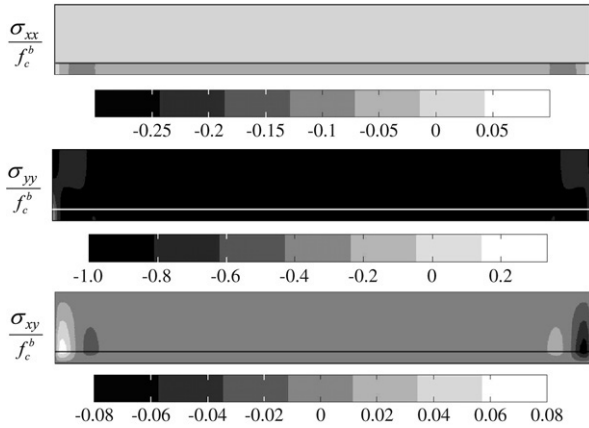
Fig. 2. Stress components at the limit state.

regular orthogonal grid having P rows and Q columns in both the mortar and the brick domain; inequality (10) is imposed to the corresponding Q points at the interface $\mathscr{S}$. Lower bound approximations N_c of the limit axial force for given eccentricity e are obtained as solutions of the LP problem

$$\begin{cases} N_c = \max N = \max \left(\mathbf{c}^{\mathrm{T}} \mathbf{z} \right) = \max \left(z_0 \int_{-\frac{d}{2}}^{\frac{d}{2}} f_0'' \, \mathrm{d}x \right) \\ \qquad \mathbf{S z = 0} \\ \qquad \mathbf{M z \leq d} \\ \qquad \mathbf{Q z \leq 0}, \end{cases} \tag{11}$$

where matrices $\mathbf{S}$, $\mathbf{M}$ and $\mathbf{Q}$ are related to the conditions of stress continuity at the interface $\mathscr{S}$, plastic admissibility according to the piecewise linearization of the Mohr–Coulomb limit domain and unilateral frictional contact at the interface $\mathscr{S}$, and vector $\mathbf{c}$ is defined in (11)a [31].

The procedure is applied to the case of concentric loading assuming a brick stack with $d = 250$ mm, $h_b = 55$ mm, $h_m = 10$ mm. Non-dimensional polynomial functions are assumed as:

$$g_s^m (y) = \left(\frac{2y}{h_m} \right)^{2(s-1)}, \quad s = 1, \ldots, S_\alpha, \tag{12a}$$

$$g_s^b (y) = \left(\frac{2 (h_m + h_b - y)}{h_b} \right)^{2(s-1)} \quad s = 1, \ldots, S_\alpha, \tag{12b}$$

and

$$f_r (x) = \left(\frac{2x}{d} \right)^{r-1} \left[\cos \left(\frac{2\pi}{d} x \right) + 1 \right], \quad r = 1, \ldots, R. \tag{12c}$$

As the result of a convergence analysis to limit the error within 0.1%, parameters R, S, K, P and Q have been given the values: $R = 16$, $S = 6$, $K = 30$, $P = 240$, $Q = 20$. The material strength is chosen in the typical range for brittle materials, $f_t^b / f_c^b = 1/10$, $f_t^m / f_c^m = 1/10$, $f_c^m / f_c^b = 1/4$, $\mu = 0.2$, resulting in a brickwork compressive strength $f_M = 0.848 f_c^b$.

The stress field at the limit state is shown in Fig. 2. The typical stress field of the unbounded layered model is obtained in the central region, with a uniform compressive horizontal stress ($\sigma_{xx}^a < 0$) in the mortar and tensile horizontal stress ($\sigma_{xx}^b > 0$) in the brick, while close to the edges a perturbation of the stress field components is observed both in the bricks and in the mortar. The collapse condition attained in Fig. 2 is that of transverse traction in the brick but no collapse mechanism can be identified since this would ask the problem to be solved also in terms of displacements, which is beyond the scope of this work.

The relevance of the edge effects can be discussed comparing the compressive strength f_M for prisms of finite width, discussed in the previous parts of this section, in the case of concentric loading, to the strength $\tilde{f}_M$ of an unbounded layered material. The standard assumptions of Limit Analysis [3] are postulated, i.e. that, in the unbounded layered material:

(i) both the materials are in Limit condition, the mortar layer being in a three-axial compressive stress state and the brick in a three-axial tensile-tensile-compressive state; besides, Mohr–Coulomb limit conditions are attained simultaneously in both the materials;

(ii) compatibility is guaranteed, i.e. no sliding takes place at the brick/mortar interface, since no shear stresses need to be postulated in an unbounded layered material, as already discussed;

(iii) plain strain conditions.

On these bases, a generalized expression of the Hilsdorf formula [3] can be obtained assuming for the mortar the limit condition:

$$\sigma_v = -f_c^m + \frac{f_c^m}{f_t^m} \sigma_h, \tag{13}$$

being σ_v the mean component (vertical) of the compressive stress, σ_h the horizontal confining stresses, and f_c^m and f_t^m the mortar uniaxial compressive and tensile strength:

$$\tilde{f}_M = \frac{h_b \frac{f_c^m}{f_t^m} f_t^b + h_m f_c^m}{h_b \frac{f_c^m}{f_t^m} f_t^b + h_m f_c^b} f_c^b, \tag{14}$$

where the symbols have been already defined in the previous paragraphs. The Hilsdorf formula can be obtained as a specific case assuming $f_c^m / f_t^m = 4.1$ [3]. Eq. (14) does not depend on the friction coefficient at the interface because of the assumption (ii).

With respect to the unbounded layered material, the perturbation in the stress field is due, in general, to a couple of reasons: (i) the head joints; (ii) to edge effects. In the considered brickwork prisms, the first issue is not dealt with, while the effect of the latter appears to be rather limited; Fig. 3 shows that the difference due to the edge effects never exceeds 3.5% for brickwork prisms of ordinary width ($d \geq 100$ mm) and approximates 10% only for unrealistic narrow prisms ($d \leq 50$ mm).

Fig. 3 shows a comparison between the two approaches for the ratios of the material strength previously discussed, that might be unfit for some kinds of brickworks, and for increasing width d of the specimen. The brick height h_b is 55 mm, so that, varying the width d, Fig. 3 also shows the effect of the ratio h_b / d.

The effects of the mechanical and geometrical parameters of the model herein developed are showed in Figs. 4 and 5, where it is showed that the same conclusions can be derived also for different values of the mechanical and geometrical parameters.

A sensitivity analysis of the model for $e = 0$ has been carried out. Different values of the friction coefficient in the range $\mu \in [0.05, 0.6]$ have shown no effect on the axial strength, showing that sliding at the brick/mortar interface: (i) is locked on the average by the high vertical stresses; (ii) might be activated in some areas, due to some stress concentrations, but plays a minor role on the global collapse phenomenon.

The evaluation of lower bounds to the limit axial strength $N_c (e)$ for given eccentricity e have been carried out for the same specimen. Different values of the eccentricity has been considered showing the edge effects on the stress field at the limit state; the distribution of the vertical stresses σ_{yy} is shown, Fig. 6.

The dependence of the limit axial strength N on the eccentricity is represented in the non-dimensional domain of Fig. 7 in terms of the ratios N/N_0 and M/M_0, where N_0 is the concentric limit
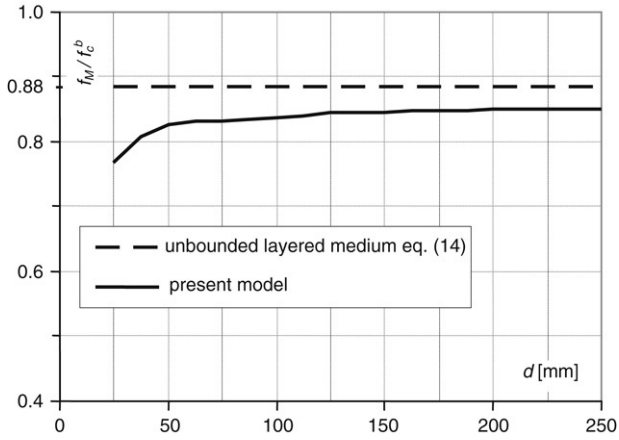
Fig. 3. Non-dimensional limit concentric axial strength f_M/f_c^b for varying the stack width (concentric loading, $e = 0$).
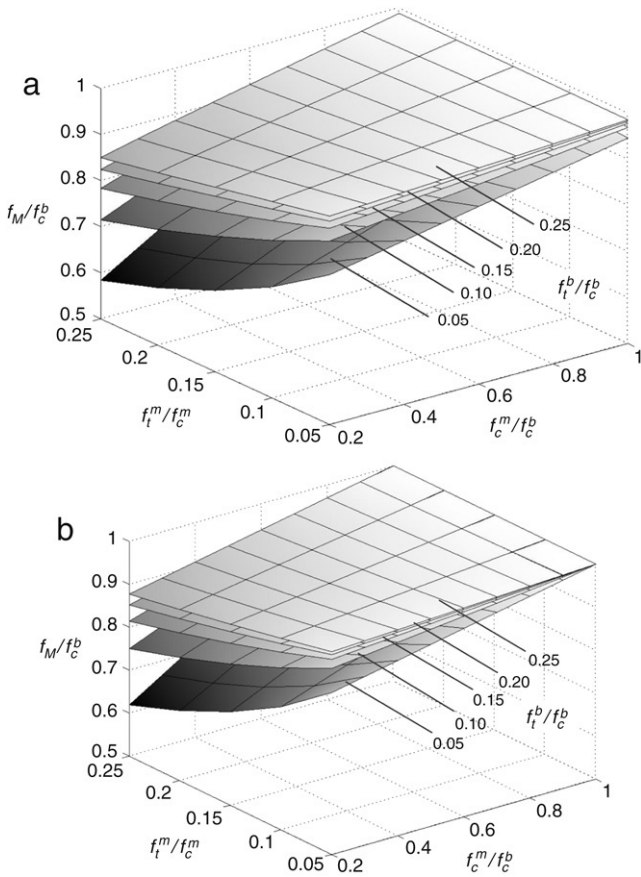

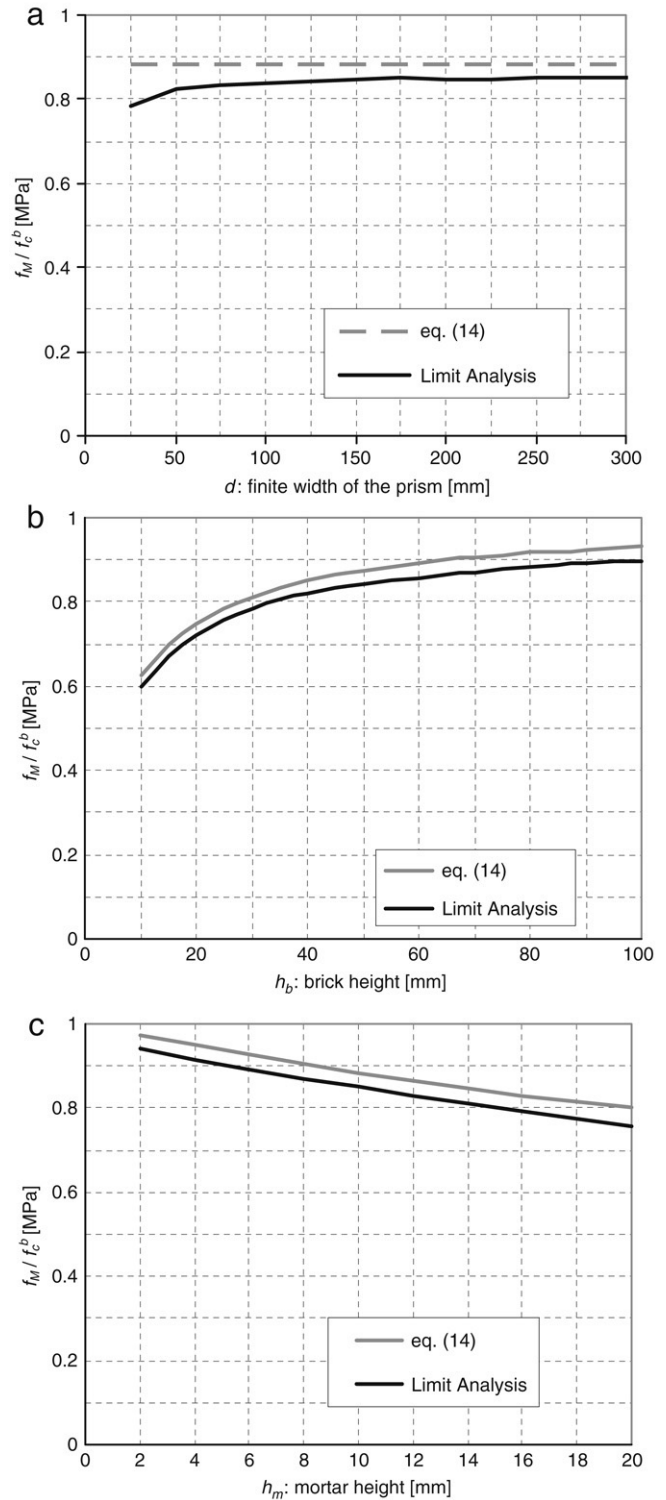**Fig. 4.** Compressive strength of brickwork as a function of the mechanical parameters. (a) prisms of finite width; (b) unbounded layered model (concentric loading, $e = 0$).

Fig. 5. Compressive strength of brickwork as a function of the geometrical parameters. (a) prisms of finite width; (b) and (c) unbounded layered model (concentric loading, $e = 0$).

load for unit thickness ($N_0 = d f_M$) and the conventional bending moment $M_0 = N_0 d/4$, the black squares in the diagram defining the limit states obtained by the present analysis. In the same diagram the limit states obtained for the homogeneous rectangular Euler-Bernoulli beam made up with no-tensile resistant (NTR) and elastic-perfectly plastic in compression material are shown, corresponding to the parabola $M/M_0 - 2N/N_0(1 + N/N_0) = 0$. The comparison highlights negligible differences between the results provided by the two models, thus suggesting that no overstrength can be postulated in case of eccentric loading, i.e. that the brickwork strength does not depend on the loading conditions.

Similar results have been obtained for varying both the value of the ratio $(h_b + h_m)/d \in [0.2, 2]$.

The obtained results, referred to both concentric and eccentric axial compression, show that, under the aforementioned assumptions: (i) the free-edge effects do not affect the concentric axial strength provided by the simple unbounded layered model; (ii) the limit eccentric axial load can be evaluated by the homogeneous
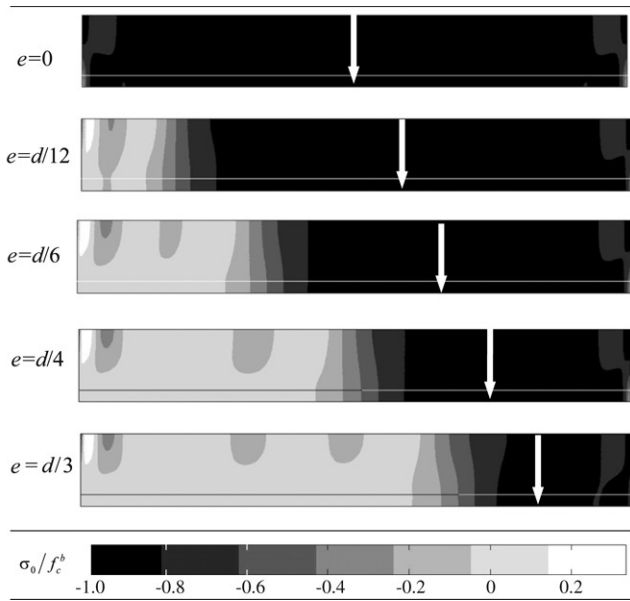
Fig. 6. Vertical stresses σ_{yy} component for varying eccentricity e.
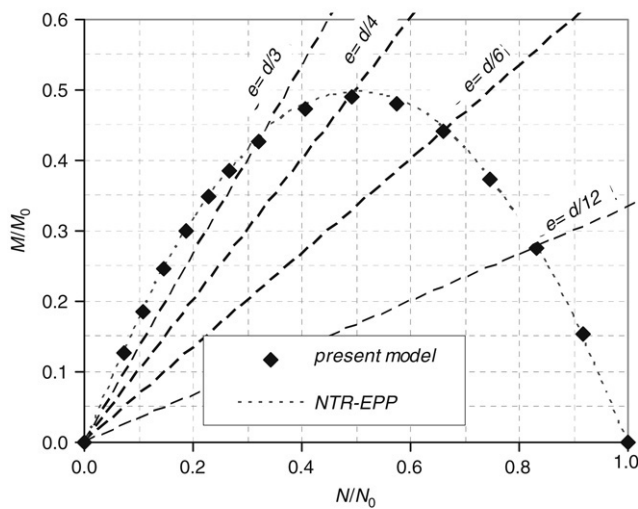

Fig. 7. Limit domains in the non dimensional plane N/N_0, M/M_0. Dots: points on the limit domain calculated according to the proposed model; dotted line: limit domain for a No Tensile Resistant – Elastic Perfectly Plastic (NT-EPP) homogeneous equivalent beam.

beam model assuming a no-tensile resistant material with ideal plastic compressive response with compressive strength deduced from concentric tests. This outcome has to be considered as a first result to be compared with others referred to more complex constitutive models since it relies on the assumption of perfect plasticity in compression, which is necessary for Limit Analysis to be applied but is somewhat strong for quasi-brittle materials such as clay bricks and mortar.

3. Tests on compressed prisms

3.1. The experimental program

Two types of specimens have been tested: (i) type 1: 110 × 250 × 270 mm, four bricks layers and five mortar joints; (ii) type 2: 250 × 250 × 345 mm, five brick layers and six mortar joints, the central level being a symmetry plane, Fig. 8. The materials
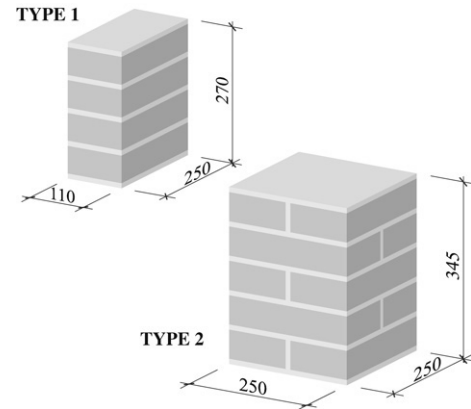

Fig. 8. Tested specimens.

have been characterized according to [32,33], Table 1, showing the dispersion of the data typical of brickwork, somewhere in-between 15% and 20% of the average value [34–36]. Mortar 1 is a cement-lime mortar and mortar 2 is a "white cement"-lime-mortar, that are industrial pre-mixed products for which the producer did not give the exact proportions, both representing medium-high strength mortars. Brickwork 1 and Brickwork 2 originate from the corresponding mortars.

The brickwork specimens have been tested with a load eccentricity of 0, 40, 60 and 80 mm (e/d = 0, 4/25, 6/25, 8/25), Fig. 9, repeating each test two or three times. Fig. 9 shows also the position where displacements have been measured for both the specimen types.

The standard tests [32,33] for the compressive and tensile strength of brick and mortar, f_c^m, f_c^b, f_t^m and f_t^b, make use of an experimental setup where friction between the specimens and the testing machine is not removed. Since friction between the specimens and the testing machine is not vanishing, in standard tests the stress state in the specimen is not uniaxial. On the contrary, the values for f_c^m, f_c^b, f_t^m and f_t^b used for both the compressive strength of brickwork, according to relationships like Eq. (14), and for characterizing the materials refer to a uniaxial stress state: therefore, the standard tests do not directly provide the uniaxial tensile and compressive strengths of the tested materials and some correction factor needs to be applied.

The application of the Limit Analysis procedure discussed in Section 2 to the compressive tests and of FEM procedures to the Three Point Bending (TPB) tests shows that the measured values are approximately 30% higher than the values that would be obtained in frictionless tests [31]; similar results would be obtained by means of 3D FEM models. Table 1 shows the uniaxial strengths of bricks and mortars.

3.2. The experimental setup

The testing setup is represented in Fig. 10. The load is applied to the specimens by means of 60 mm thick steel plates and to the plates by cylindrical hinges, and is measured by means of a C5 class *HBM-RTN* load cell with a 0.01% precision located in-between the upper plate and the testing frame (not represented in Fig. 10). The cylindrical hinges allow the load path inside the specimen to be precisely identified; different loading systems may originate undesired and not constant eccentricities of the load leading to results that are difficult to be interpreted [22].

The relative displacements between the steel plates are measured by MACH B10 Solartron® LVDTs with a 1/1200 mm precision. The displacement of the upper plate is measured directly under the load line, while the lateral ones are recorded close to

Table 1
Mechanical characteristics of bricks and mortars

	Av. value (MPa)	N. of samples	C.o.V. (%)	Char. value[a] (MPa)	Char. / average
Brick					
Compressive strength – direct	13.8	20	17	9.9	0.72
Elastic modulus (compression)	1530	20	30	765	0.50
Tensile strength – TPB	3.3	10	10	2.7	0.83
Elastic modulus (tensile)	920	10	25	535	0.58
Mortar 1					
Compressive strength – direct	9.2	20	18	6.4	0.70
Elastic modulus (compression)	1545	20	16	1130	0.73
Tensile strength – TPB	2.4	10	15	1.8	0.75
Elastic modulus (tensile)	1120	10	19	765	0.68
Mortar 2					
Compressive strength – direct	7.0	20	16	5.1	0.73
Elastic modulus (compression)	1365	20	22	865	0.63
Tensile strength – TPB	1.9	10	12	1.5	0.80
Elastic modulus (tensile)	870	10	23	535	0.62

[a] Assuming a Gaussian distribution.
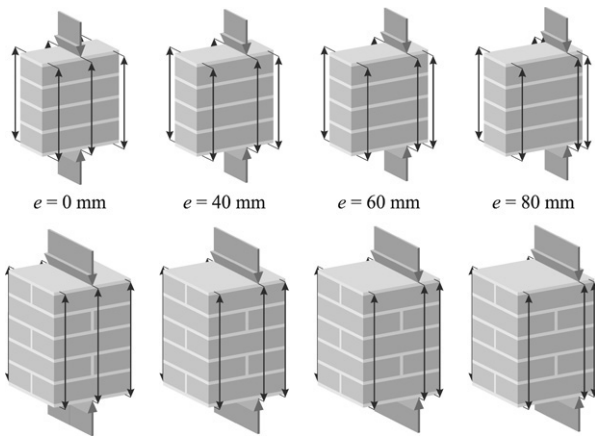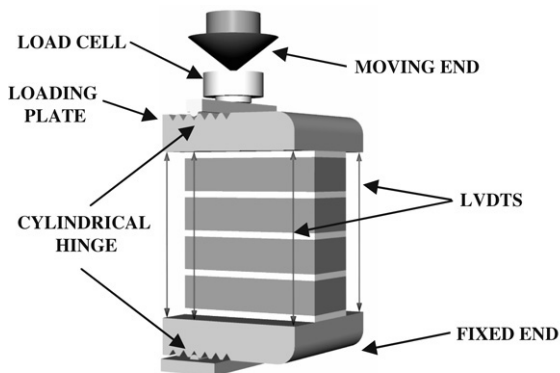

Fig. 9. Testing program.

Fig. 10. Test setup (testing frame not represented).

the ends of the specimen in order to derive the plates rotation. All the displacements are measured on both the sides of specimen in order to control undesired lateral eccentricity of the load due to imperfect bases of the specimen.

The tests are displacement controlled — lower (fixed) hinge connected to the testing frame and upper part of the reaction frame (above the load cell) moved by a mechanical device. The load cell can be considered a stiff spring; up to the limit load this does not affect the results and could be somehow relevant only far after the material collapse, at a point when the softening curve has already lost any mechanical meaning. A 2 mm thick lead sheet between the

specimen and the loading plates was used to smoothen the bases of the specimens. Friction between the bases and the loading plates could not be removed because eccentric loading without friction would result in unstable tests.

For type 2 specimens, due to the higher loads expected, the tests have been force-controlled by means of an hydraulic press with 0.7% precision. In these cases, the post-peak parts of the diagrams have been obtained stopping the oil pump and waiting till equilibrium was reached again. The displacements have been measured with the same LVDTs already described and the load through the pressure of the hydraulic system. Other minor details can be found in previously published works of the authors [17,22,31].

3.3. Test results

Figs. 11 and 12 show the load–displacement diagrams for concentric ($e = 0$) and eccentric load tests. Concentric tests show a typical response that can be divided into 4 different phases: phase (1) up to approximately 80% of the peak load the response is linear elastic; phase (2) a non linear phase is activated up to the peak load; phase (3) inelastic strains are developed at almost constant load, this phase being almost vanishing or relatively long according to the specimen type and the testing conditions; phase (4) a long softening branch lasting till the specimen crushes in several pieces, Fig. 13.

The dispersion of the data, Table 2, is reduced and well inside the known limits for brickwork [34–37]. Type 1 specimens show a more dispersed response than type 2 ones, probably because of the mortar joints of the brickwork. In type 1 specimens the joints are difficult to be completely filled since mortar leaks during the construction of the specimens; for type 2 prisms, the vertical joints help in filling the horizontal ones so that the leakage takes place close to the outer surface of the bricks only.

Figs. 14 and 15 show the moment–curvature diagrams for the eccentrically loaded specimens. Comparing these data to the load–displacement curves we can observe that: (i) the softening branch is more regular if referred to the curvature rather than to the displacements; (ii) the curvature at peak load is less dispersed than the displacement at peak load.

Fig. 16 shows the crack pattern at the end of the tests for type 1 and type 2 specimens which suggests a collapse mechanism under concentric loading that is different for the two bonds.

Type 1: the collapse mechanism is first activated by the detachment of 10 mm thick layers of the brick from the outer surface (phase 2, Fig. 13); only in a further phase the transversal tractions make the brick split into several parts (phase 3, Fig. 13).
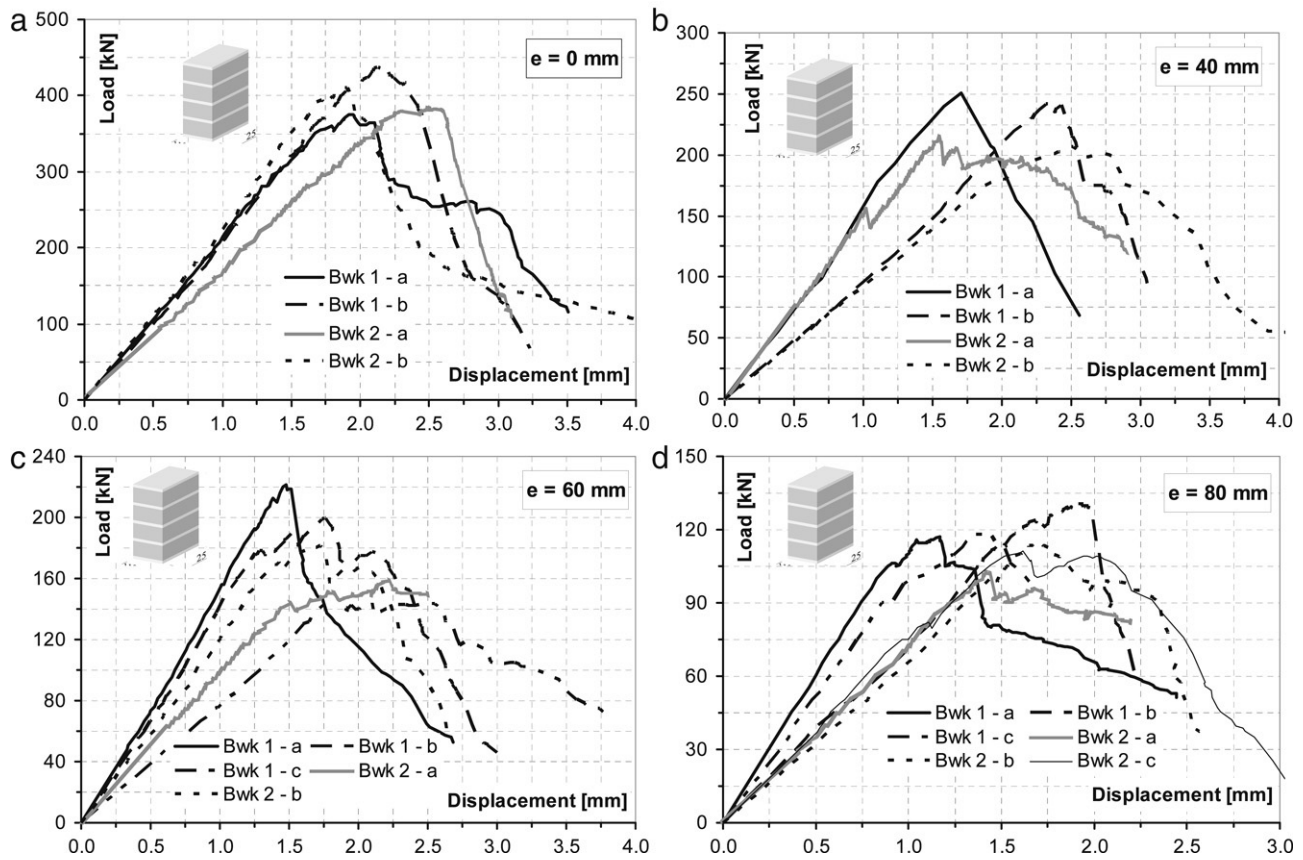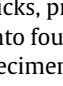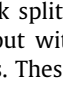
Fig. 11. Load–displacement diagrams for type 1 specimens: (a) concentric loading; eccentric loading with: (b) $e = 40$ mm ($e/d = 1/6$); (c) $e = 60$ mm ($e/d = 1/4$); (d) $e = 80$ mm ($e/d = 1/3$).

Table 2
Summary of the experimental data – concentric loading

Specimen type-n		f_M^c (MPa)	ε_{el} (%)	ε_u(%)	$\eta_{av} = \varepsilon_u/\varepsilon_{el}$	E (MPa)
Brickwork 1						
Type 1—a		12.5	0.64	0.71	1.27	1990
Type 1—b		14.5	0.60	0.79	1.51	2080
Type 1—average		13.5	0.62	0.75	1.39	2035
Type 2—a		12.4	0.47	0.65	1.42	2210
Type 2—b		12.7	0.56	0.64	1.34	2550
Type 2—average		12.5	0.51	0.64	1.38	2380
Brickwork 2						
Type 1—a		12.8	0.82	0.95	1.16	1610
Type 1—b		13.7	0.56	0.70	1.16	2200
Type 1—average		13.2	0.69	0.83	1.16	2085
Type 2—a		12.6	0.55	0.71	1.31	2120
Type 2—b		12.2	0.49	0.58	1.44	2500
Type 2—average		12.4	0.52	0.64	1.37	2310

Type 2: the first cracks appear along the interface between the vertical joints and the bricks, propagate into the bricks so that the prism is first separated into four equal brickwork pillars (each one is 1/4th of the original specimen) at approximately 50% of the limit load; then the brickwork splits in several pieces for transversal tractions in the bricks but without the detachment of external layers as for type 1 tests. These differences almost disappear for eccentric loading, for which the compressed part of the prism progressively crushes in both the cases.

In all the tests, since the friction between the plates and the specimens could not be removed, the upper and lower bases showed signs of confinement due to the friction between the specimen and the testing machine. The collapse of the specimen, being activated in the central section of the brickwork prism, is expected not to be affected by these phenomena even though the prisms are relatively short (usually 5 horizontal mortar joints are suggested for testing brickwork, but also 3 joints are considered acceptable).
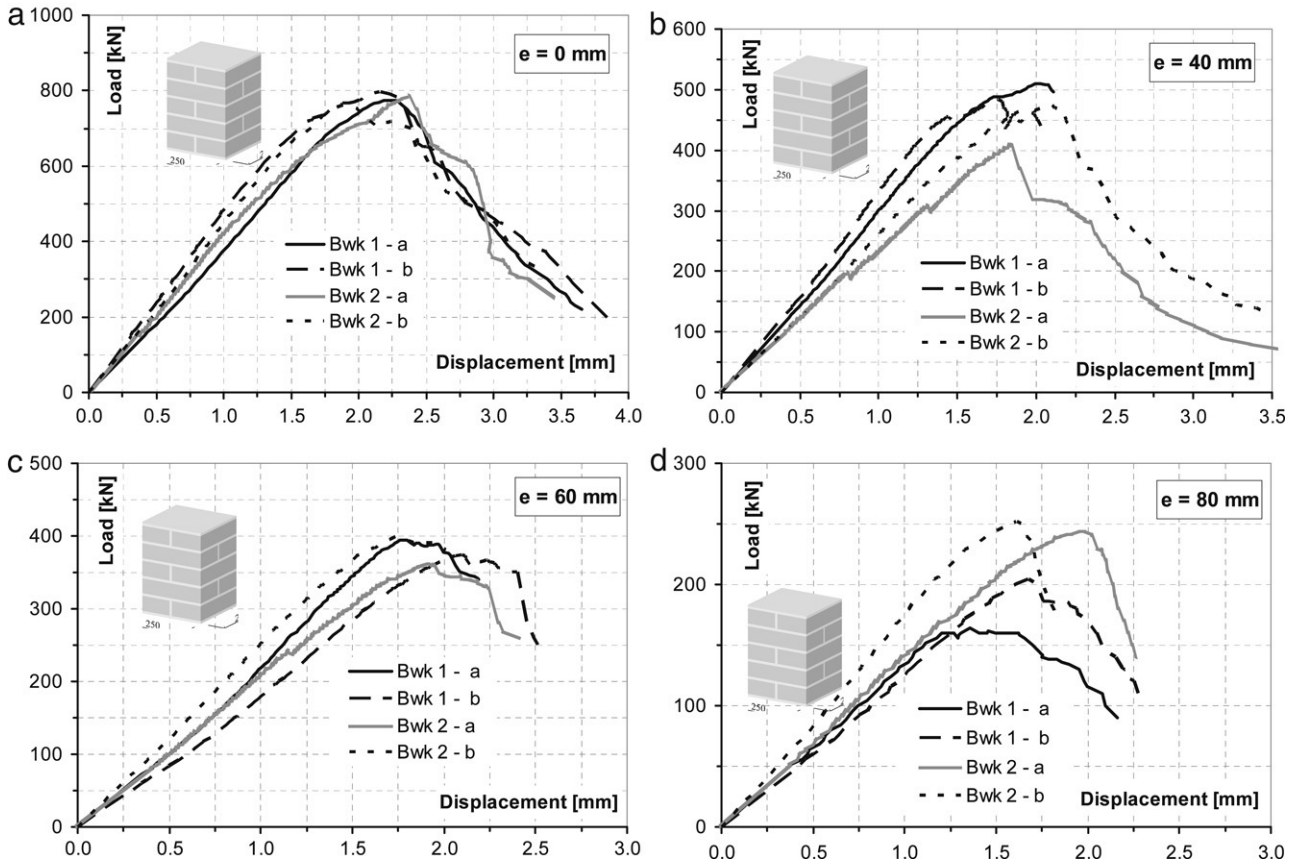
Fig. 12. Load–displacement diagrams for type 2 specimens: (a) concentric loading; eccentric loading with: (b) $e = 40$ mm ($e/d = 1/6$); (c) $e = 60$ mm ($e/d = 1/4$); (d) $e = 80$ mm ($e/d = 1/3$).
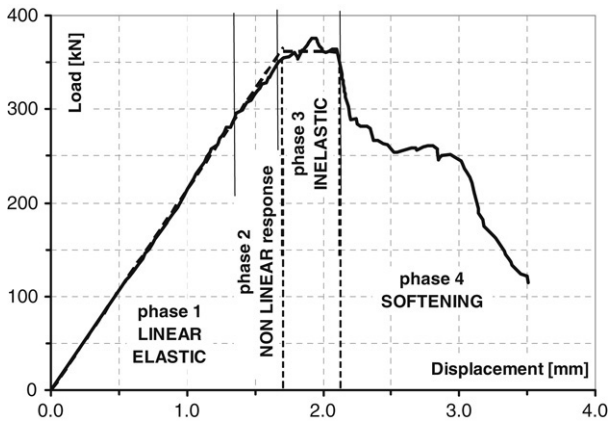

Fig. 13. Typical load–displacement response of concentrically loaded brickwork.

Aiming at the assessment of eccentrically loaded structures, the experimental data are best represented in a N/N_0–M/M_0 plane, being the normalising quantities N_0 and M_0 the ultimate load for concentric loading and $M_0 = N_0 \cdot d/4$ respectively. The model discussed in the previous paragraph, based on Limit Analysis and on the assumption that clay and mortar may be represented by Elastic–Perfectly-Plastic models with unbounded ductility, led to a limit domain represented by the parabola in the N/N_0–M/M_0 plane of Fig. 17 that includes almost all the experimental points.

The normalising quantity N_0 of Fig. 17, that is conceptually "exact" if we knew the "real" brickwork compressive strength, is defined as the average experimental value; since different types of masonry have been tested, part of the dispersion is due to the

choice of one normalising quantity only, which is necessary for direct comparison of the test data.

4. Simplified homogeneous models

The beam-like approach to the assessment of eccentrically loaded masonry asks uni-axial homogeneous models to be formulated. On the basis of the Navier hypothesis of plane section, experimentally verified for some kind of solid clay brickwork [8], several constitutive models can be formulated. Assuming a vanishing tensile strength (No-Tensile-Resistant material, NTR), several different constitutive models may be considered in compression: (i) Perfectly-Brittle (NTR-PB), Fig. 18a, or (ii) Elastic–Perfectly-Plastic (NTR-EPP), Fig. 18b, in compression. These models are simple in the sense that they require only one parameter, the compressive strength f_M, to be defined.

The Navier hypothesis of plane section and the mono-axial constitutive law make the stress distribution on the section known; the internal forces, calculated by integration of the stress distribution, therefore depend of the assumed constitutive parameters: the shape of the stress–strain response and the compressive strength f_M. In ultimate conditions, i.e. when the maximum compressive strain attains its ultimate value, a limit domain can be derived in the axial thrust-bending moment space (N–M space) that is used for the safety assessment of eccentrically loaded structures, assuming safe all the states that lie inside the domain. Since the assessment refers to the internal forces, i.e. to global quantities, the homogeneous beam-like approach does not allow the actual stress state on the cross section to be reproduced and the compressive strength f_M needs to be considered as a global strength parameter, not a local limit stress; being its
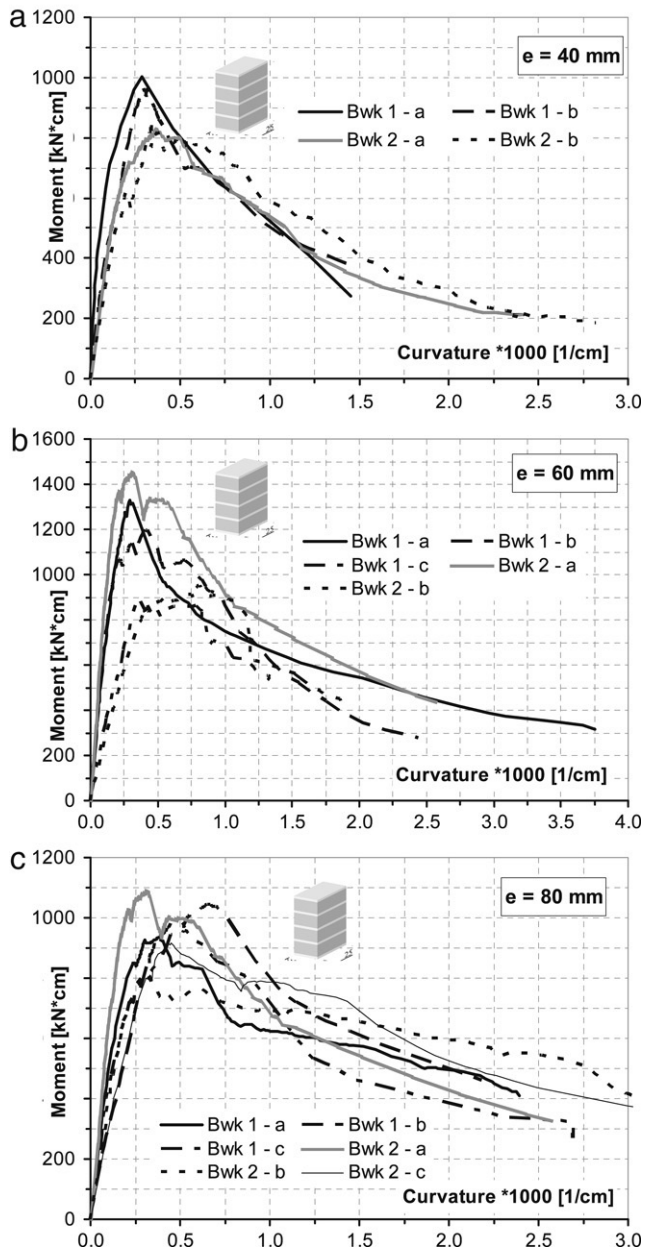
Fig. 14. Moment–curvature diagrams for type 1 specimens; eccentric loading with: (a) $e = 40$ mm ($e/d = 1/6$); (b) $e = 60$ mm ($e/d = 1/4$); (c) $e = 80$ mm ($e/d = 1/3$).
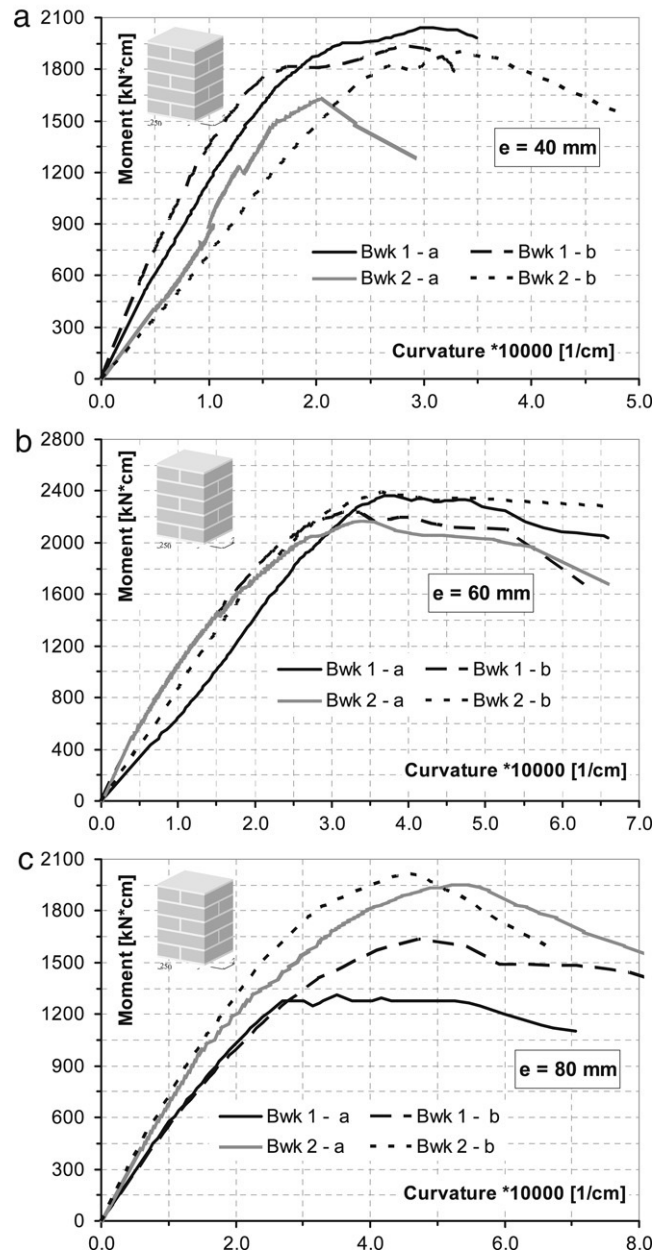

Fig. 15. Moment–curvature diagrams for type 2 specimens; eccentric loading with: (a) $e = 40$ mm ($e/d = 1/6$); (b) $e = 60$ mm ($e/d = 1/4$); (c) $e = 80$ mm ($e/d = 1/3$).

correlation to the mechanical properties of bricks and mortar not straightforward and somehow troublesome, it is defined on the basis of compressive (concentric) tests. In fact, the concept of compressive strength is not strictly necessary, since the ultimate load for concentric loading, N_0, could be only a parameter needed for the limit domain to be drawn.

The diagrams of Figs. 11 and 12 show that neither a brittle NTR-PB nor a ductile NTR-EPP model fit the actual response of brickwork and that they appear to be lower and upper bounds to the actual load carrying capacity of the cross section: the first one because it does not represent the inelastic response of brickwork, the latter model because the experimental evidence shows a rather limited inelastic capacity for masonry. On the basis of this observation, an NTR-EPP model might still be considered provided a limit is set to the inelastic strains. To this aim, two relevant parameters can be defined: the ultimate displacement δ_u just at the end of phase 3 and the elastic limit δ_{el} at the intersection between the linear

elastic phase and the inelastic plateau, Fig. 13. The ratio between the ultimate displacement δ_u and the value at the end of the elastic limit δ_{el} [17] is defined as "available ductility" $\eta_{av} = \delta_u/\delta_{el}$ and can be assumed as a measure of the material inelastic capacity. Such a definition is the same as the more common definition of ductility referred to the ultimate and elastic mean strain in the specimen, $\eta_{av} = \varepsilon_u/\varepsilon_{el}$. The meaning of the available ductility η_{av} is that of a global parameter representing the first part of the inelastic response, depending on several parameters such as the properties of the constituents, their geometry (unit size and joint thickness) and on the masonry bond. This inelastic parameter, η_{av}, can be deduced from concentric tests, Table 2.

Since the inelastic plateau is not always easy to identify, Fig. 13, the definition of available ductility leaves room for uncertainty. Even though this is an undesirable feature of a mechanical model, the practical effect of such an uncertainty remains far below the approximation of the simplified model. This constitutive model is
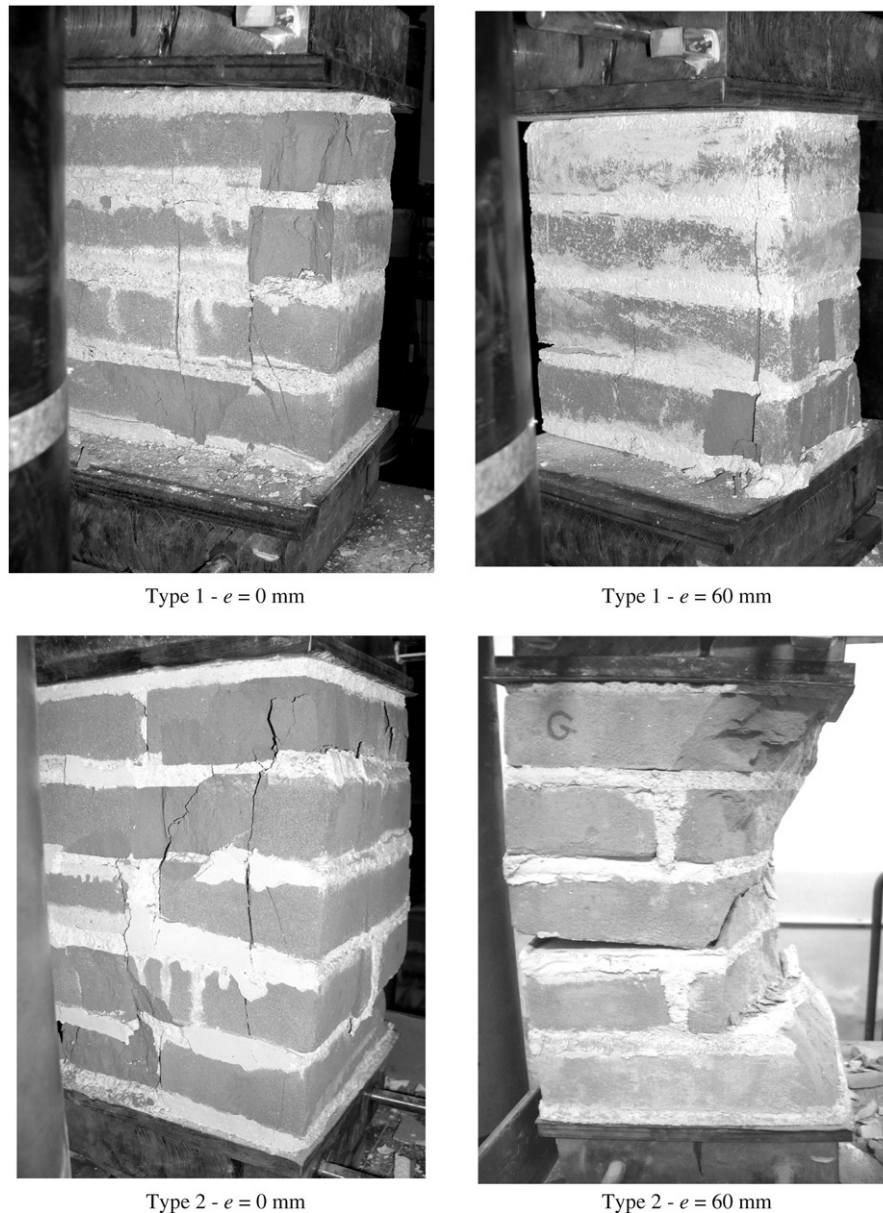
Type 1 - $e = 0$ mm

Type 1 - $e = 60$ mm

Type 2 - $e = 0$ mm

Type 2 - $e = 60$ mm

Fig. 16. Collapse mechanism for type 1 and type 2 specimens under concentric and eccentric loading.

given the name of No Tensile Resistant – Elastic Plastic – Limited Available Ductility model (NTR-EP-LAD), Fig. 18c and dashed line of Fig. 13.

Fig. 19 shows the limit domains in the N/N_0–M/M_0 plane obtained for: (i) the NTR-PB model, Fig. 18a, inner solid curve ($\eta_{av} = 1$); (ii) the NTR-EPP model, Fig. 18.b, and the Limit Analysis approach of paragraph 2, outer solid parabola ($\eta_{av} \to \infty$); (iii) the NTR-EP-LAD model for some values of η_{av} ($\eta_{av} = 1.2$, $\eta_{av} = 1.5$, $\eta_{av} = 2$). The vast majority of the experimental points lie inside the two extreme models; some points lie slightly outside these limits but this is due to the variability of the concentric compressive strength, which is the normalizing quantity. Taking into account a $+10\%$ and -10% variation of the compressive strength, i.e. somehow taking into account the material inhomogeneity, we obtain the outer dashed and inner dotted lines, that contain all the experimental points.

The limit domain for the NTR-PB model, on principle, cannot be considered a lower bound to the brickwork strength since local stress concentrations in masonry and the quasi-brittle response of the constituents and interfaces might lead to failure domains

also more restricted than the ones predicted by this model. Nevertheless, for the considered cases, no experimental test falls inside the NTR-PB safe area, Fig. 19, so that it can be assumed, for practical applications, as a lower bound to the brickwork load carrying capacity under eccentric loads.

Several points show very limited ductility, while the majority of the experimental tests would be interpreted by an NTR-EP-LAD model assuming the available ductility η_{av} in the range [1.2, 1.5], as deduced from the concentric tests of Table 2. For different mortar types and thicker mortar joints, ductility may be as large as 2 [22,38].

5. Discussion

In this paper a first approach to solid clay brickwork has been discussed, assuming for brickwork masonry a simple stacked model with finite width. This model, whatever simple, allows the edge effects to be taken into account as opposed to other models classical models [3] that consider brickwork as an unbounded layered material. Static Limit Analysis has been applied to derive
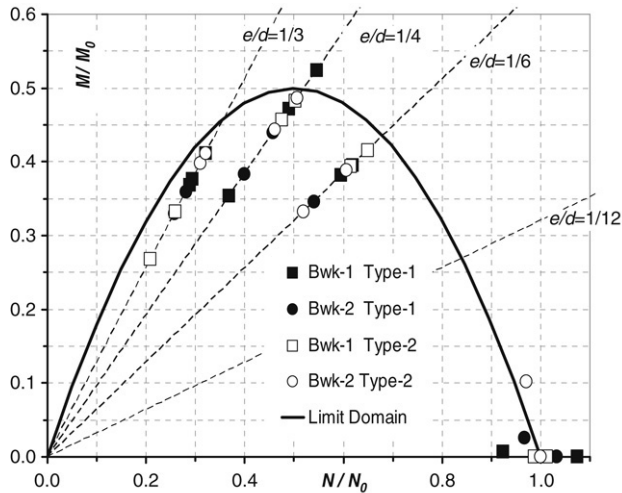
Fig. 17. Limit domain of the NTR–EPP model and experimental points in the N/N_0–M/M_0 plane.

the load carrying capacity of the material for both concentric and eccentric loading, Fig. 7; the obtained limit domain and the limit curve for a simplified homogeneous perfectly-plastic model are almost coincident showing that the edge effects seem to play a minor role (not more than 3.5%) on the collapse of solid clay brickwork.

The test data and the comparison with the theoretical results show that the Limit Analysis approach of paragraph 2 overestimates the actual load carrying capacity of the material, which is likely to be due to the damage and fracture inelastic phenomena taking place in clay and mortar and/or at their interface prior and close to the peak load; these phenomena are not taken into account by Limit Analysis Procedures. In fact

this outcome is not completely unexpected since masonry and its constituents are not ductile materials, while Limit Analysis assumes the materials to be ductile in order to reach the limit conditions in all the materials of the model.

The latter conclusion is relevant to assessment procedures: since assessment asks no permanent strain (damage) to be admitted, the limit domain considered for assessment should be the brittle one, i.e. the inner curve of Fig. 19, calculated with the NTR-Perfectly Brittle model of Fig. 18a.

Type 1 specimens, with horizontal joints only, allow a direct comparison between the theoretical estimate of the limit load under concentric loading, Eq. (14), and the experimental value, Table 3, showing good agreement between theoretical and test data, with differences falling inside the scattering of experiments [35,36]. Similar results are obtained also for type 2 specimens that, due to the head joints, do not exactly fit the assumptions of the previously discussed model.

The Hilsdorf model [3] differs from Eq. (14) because: (i) the ratio f_c^m/f_t^m is assumed constant and equal to 4.1; (ii) a reducing factor $1/U$ is introduced (1/1.5 for solid brickwork) to take into account the inhomogeneity of the stress field. In fact, if the uniaxial material strength is considered in Hilsdorf formula, no correction factor U needs to be used to fit the experimental data; the difference in the compressive-to-tensile strength ratios plays a minor role.

The limit domain is usually deduced from simplified homogenised beam-like models that assume for the material the uniaxial constitutive laws discussed in Section 4 or other similar models. In this case, the compressive strength is considered a material parameter either measured through concentric load tests or provided by theoretical approaches, in both the cases assuming a uniform distribution of compressive stresses. The UIC railway code [23], on the contrary, assumes a NTR-PB model for the assessment of masonry bridges providing the compressive strength under eccentric loading $f_M^{eccentric}$ as a function of the value for concentric
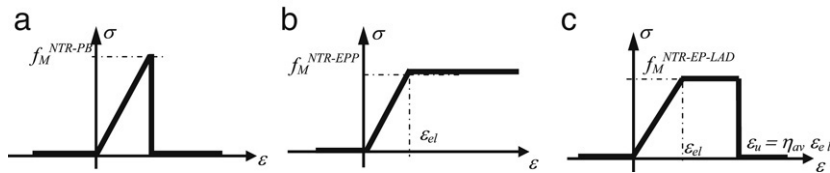

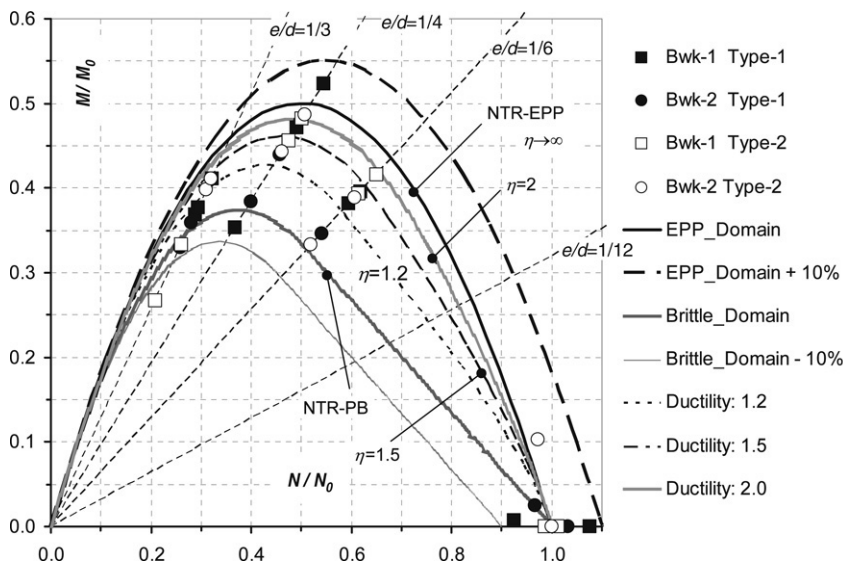**Fig. 18.** Uniaxial constitutive models for masonry; (a) NTR-PB, (b) NTR–EPP; (c) NTR-EP-LAD models.

Fig. 19. Limit domain of the NTR-PB, NTR–EPP and NTR-EP-LAD models and experimental points in the N/N_0–M/M_0 plane.

Table 3
Compressive strength f_M of the tested brickwork: experimental and theoretical values [MPa]

Brickwork 1—type 1 prism			Brickwork 2—type 1 prism		
Exp.	Eq. (14)	Limit analysis Section 2	Exp.	Eq. (14)	Limit analysis Section 2
12.5 **14.5**	13.0	12.5	**12.8** **13.7**	12.6	12.2

Table 4
Ultimate load and compressive strength of all the specimens for different constitutive models

Brickwork 1

	0 mm		40 mm		60 mm			80 mm		
Eccentricity Eccentr. /brick height	$e/d = 0$		$e/d = 1/6$		$e/d = 1/4$			$e/d = 1/3$		
Specimen	a	b	a	b	a	b	c	a	b	c
N_u^{exp} (kN)	375	436	251	242	221	199	150	117	131	119
f_M^{NTR-PB} (MPa)	12.5	14.5	16.4	15.8	18.9	17.0	12.8	14.4	16.2	14.7
			Average: 16.1		Average: 16.2			Average: 15.1		
$f_M^{NTR-EP-LAD}$ (MPa) ($\eta_{av} = 1.2$)	Average: 13.5		14.4	13.9	16.6	14.9	11.2	12.7	14.2	12.9
			Average: 14.1		Average: 14.2			Average: 13.3		

Brickwork 2

	0 mm		40 mm		60 mm		80 mm		
Eccentricity Eccentr. /brick height	$e/d = 0$		$e/d = 1/6$		$e/d = 1/4$		$e/d = 1/3$		
Specimen	a	b	a	b	a	b	a	b	c
N_u^{exp} (kN)	384	410	214	206	158	181	102	115	111
f_M^{NTR-PB} (MPa)	12.8	13.7	14.9	13.4	13.5	15.5	12.6	14.2	13.7
			Average: 14.2		Average: 14.5		Average: 13.5		
$f_M^{NTR-EP-LAD}$ (MPa) ($\eta_{av} = 1.4$)	Average: 13.2		11.6	11.1	11.2	12.8	10.4	11.7	11.3
			Average: 11.3		Average: 11.5		Average: 11.1		

Type 1 specimens.

loading $f_M^{concentric}$ and of the load eccentricity e:

$$f_M^{eccentric} = \left[1.8 - 1.2 \left(1 - 2\frac{e}{d} \right) \right] f_M^{concentric},$$

$$\text{provided } \frac{e}{d} \in \left[\frac{1}{6}, \frac{5}{12} \right], \tag{15}$$

being d the section height. Eq. (15) accounts for a 60% increase of the compressive strength for the highest values of the load eccentricity. The subsequent limit domain in the N/N_0–M/M_0 plane is showed in Fig. 20 where, for high values of load eccentricity, the limit domain turns out to be enlarged. The comparison with the experimental data of this research and from other works [10–14,17–19,22] shows that several collapse points (highly eccentric loads) lie inside what the UIC approach assumes as a safe area. Since high eccentricities of the axial thrust are to be expected close to the collapse of masonry arches and arch barrels, Eq. (15) is found to be unconservative for these structures. It is worthwhile noting that Euro Code 6 [24] does not allow any strength increase at all.

Table 4 summarizes part of the data of this research and the values of the compressive strength derived from the homogeneous NTR-PB model (f_M^{NTR-PB}), Fig. 18a, and for the NTR-EP-LAD model ($f_M^{NTR-EP-LAD}$) of Fig. 18c; only type 1 specimens are considered due to the assumption of stacked periodic material on which the theoretical model is based. In spite of the data scattering, a strength increase seems to be found in the first case (brittle model) while the latter model, taking into account the available ductility measured in concentric tests, Table 2, does not need any strength increase. Assuming a NTR-EP-LAD model, brickwork 1 would be given a compressive strength of 12.9 N/mm² and C.o.V. = 12%, while for brickwork 2 of 12.0 N/mm² and C.o.V. = 7%.

The difference between these two constitutive models is due to some intrinsic features of concentric and eccentric tests: (i) concentric tests produce a uniform stress distribution in the specimen, leading to a statically determinate problem for which the average compressive strength f_M may be easily defined; (ii)

eccentric loads induce a stress distribution which is unknown, leading to a statically indeterminate problem that allows the compressive strength to be calculated only if compatibility conditions for the strains of the section and a constitutive model for the material are assumed. The NTR-PB model, neglecting the inelastic strains, needs an increase of compressive strength f_M^{NTR-PB} to be postulated; the mechanical origins of such an increase would remain unexplained.

6. Concluding remarks

The assessment of eccentrically loaded masonry structures, such as arches and pillars, is usually performed assuming simplified homogenised constitutive models for masonry according to the standard approach to r.c. elements. Since masonry is a heterogeneous material, the validity limits of such an approach need to be carefully investigated.

In this paper a first approach to this problem has been discussed on the basis of a theoretical model for periodic solid clay brickwork. It is showed that, in the frame of the considered brick stacked prisms/geometry, the local perturbations of the stress field, due to free edge effects, seem to play a minor role on the brickwork collapse, making the compressive strength to be related to the mechanical properties of brickwork constituents and to the size of bricks and mortar joints only. These outcomes are affected by the basic assumption needed for Limit Analysis to be applied, such as the perfect plastic compressive response of the materials, that is somewhat questionable for quasi-brittle materials such as brick and mortar. Nevertheless, such an approach provides a first deep insight into the phenomena leading to the collapse of solid clay brickwork and into the free edge effects. Whatever the objection in principle, such an approach is substantiated by the experimental data collected from a series of eccentric load tests on brickwork prisms.

The experimental results provide information on the failure mechanism and on the reliability of simplified homogenised
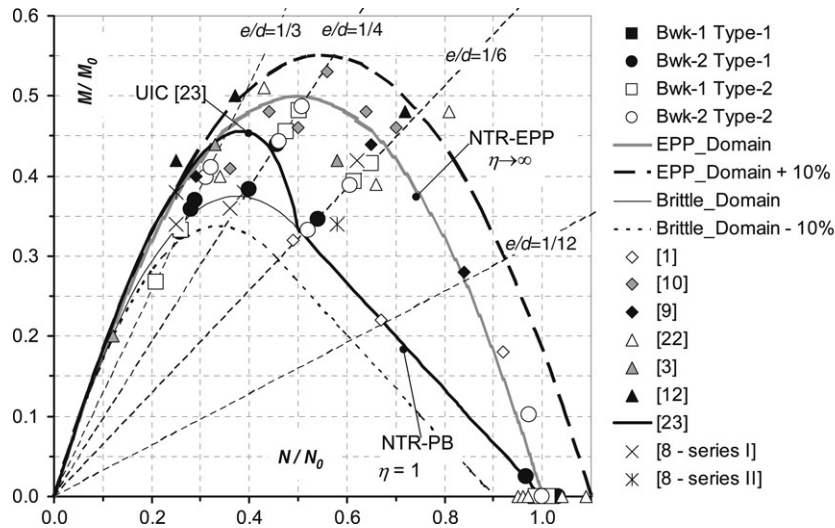
Fig. 20. Limit domains of the NTR–models, experimental data and enlarged UIC [23] domain.

models for masonry. In spite of the data scattering, which is typical of masonry structures, the NTR homogenised approaches are showed to be a practical tool for the assessment of eccentrically loaded brickwork.

Even though the theoretical approaches needs to be extended to other brickwork bonds, taking into account also the vertical head joints, and the experimental data base needs to be widened, it can be argued that the strength increase related to load eccentricity, that needs to be postulated in a NTR-PB model to fit the test results, is not a physical phenomenon but an analytical outcome due to excessively simplified approaches to eccentrically loaded sections. Similar conclusions have been derived on solid clay brickwork [17, 18,22] and by Cavaleri et al. [19] on tuff stone brickwork. According to this result, a conservative approach to the assessment of arch-type structures, and any design code provision, should neither consider a strength increase for eccentric loads nor should allow any inelastic strain to be developed.

The extension of the present analysis to other brickwork bonds, not considered by the present theoretical and experimental work, is needed to estimate the influence of bricks and mortars (geometrical and mechanical properties), of the bond pattern and of the load eccentricity on the load carrying capacity of the masonry prisms. These outcomes will be able to evaluate and possibly confirm the reliability of the simplified homogenised models to massive brickwork elements, such as the arch barrels and piers of masonry bridges and thick arches and vaults.

Acknowledgments

References

[1] Lourenço PB, Pina Henriquez J. Validation of analytical and continuum numerical methods for estimating the compressive strength of masonry. Comp Str 2006;84:1977–89.
[2] Lourenço PB, Zucchini A. Mechanics of masonry in compression: Results from a homogenisation approach. Comp Str 2007;85:193–204.
[3] Hilsdorf HK. Investigation into the failure mechanism of brick masonry under axial compression. In: Johnson FB, editor. Proc. of designing, eng.ng & constr. with masonry products. Houston (Texas): Gulf Publishing; 1969.
[4] Francis AJ, Horman CB, Jerrems LE. The effect of joint thickness and other factors on the compressive strength of brickwork. In: Proc. 2nd I. B. MA. C. Stoke on Kent. 1971.
[5] Khoo CL, Hendry AW. A failure criteria for brickwork in axial compression. In: Proc. 3rd I.B.Ma.C. Essen. 1973. p. 141–5.
[6] Atkinson RH, Noland JL. A proposed failure theory for brick masonry in compression. In: Proc. of the 3rd Can. mas. symp. Edmonton; 1983.
[7] Rots JG. Numerical simulation of cracking in structural masonry. Heron; 1991. p. 36.
[8] Biolzi L. Evaluation of compressive strength of masonry walls by limit analysis. J Struct Eng 1988;114:2179–89.
[9] Milani G, Lourenço PB, Tralli A. Homogenised limit analysis of masonry walls. Part I: Failure surfaces. Part II: Structural examples. Comp Str 2006;84:166–95.
[10] Hatzinikolas M, Longworth J, Warwaruk J. Failure modes for eccentrically loaded concrete block masonry walls. ACI J 1980;77:258–63.
[11] Drysdale RG, Hamid AA. Capacity of concrete block masonry prisms under eccentric compressive loading. ACI J 1979;80:707–21.
[12] Drysdale RG, Hamid AA. Effect of eccentricity on the compressive strength of brickwork. J Brit Cer Soc 1982;30:102–8.
[13] Drysdale RG, Hamid AA, Baker LR. Masonry structures, behaviour and design. Englewood Cliffs: Prentice Hall; 1993.
[14] Martinez JLM. Theoretical and experimental determination of the limit domains of masonry structures, and application to historical structures. Ph.D. thesis. Madrid (Spain): T. U. of Madrid; 2003 [in Spanish].
[15] Martin Caro JA. Masonry compressive strength enhancement under eccentric axial load. In: Roca, Molins editors Proc. 4th arch bridge conf., 2004: CIMNE. Barcelona. 2004. p. 405–12.
[16] Roberts TM, Hughes TG, Dandamudi VR, Bell B. Quasi-static and high cycle fatigue strength of brick masonry. Const Build Mat 2006;20:603–14.
[17] Brencich A, Gambarotta L. Mechanical response of solid clay brickwork under eccentric loading. Part I: Unreinforced masonry. Mat Str (RILEM) 2005;38: 257–66.
[18] Maurenbrecher AHP. Compressive strength of eccentrically loaded masonry prisms. In: Proc. of the 3rd can. mas. symp., 1983. p. 10/1–10/13.
[19] Cavaleri L, Failla A, La Mendola L, Papia M. Experimental and analytical response of masonry elements under eccentric vertical loads. Eng Str 2005; 27:1175–84.
[20] Castigliano CAP. Theorie de l'equilibre des systeme elastique et ses application. Negro ed.: Torino; 1879.
[21] De Felice G. Experimental behaviour of brick masonry under axial load and bending. In: Proc. 7th int. mas. conf. 2006.
[22] Brencich A, De Felice G. Eccentric loading of solid clay brickwork: Experimental results and macroscopic models. Constr Build Mat 2007 [submitted for publication].
[23] UIC—International Union of Railways: UIC code 778-3R. Recommendations for the assessment of the load carrying capacity of the existing masonry and mass-concrete arch bridges; 1995.
[24] ENV 1996-1-1. EURO CODE 6. Design of masonry structures, Part 1-1: General rules for buildings—Rules for reinforced and un-reinforced masonry; 1998.
[25] Heyman J. The stone skeleton. Int J Sol Str 1966;2:249–79.
[26] Heyman J. On shell solutions for masonry domes. Int J Sol Str 1967;3:227–41.
[27] Oppenheim IJ, Gunaratnam DJ, Allen RH. Limit state analysis of masonry domes. J Struct Eng ASCE 1988;115(4):868–82.
[28] Como M. Equilibrium and collapse analysis of masonry bodies. Meccanica 1992;27(3):185–94.
[29] Timoshenko SP, Goodier JN. Theory of elasticity. 3rd ed. McGraw-Hill Publishing C.; 1970.
[30] Sloan SW. Lower bound limit analysis using finite elements and linear programming. Int J Numer Anal Methods Geomech 1988;12:61–7.

[31] Corradi C. Theoretical and experimental analysis of the strength of eccentrically loaded brickwork. Ph.D. thesis. Italy: Dept. of Str. and Geotech. Eng.ng, Univ. of Genoa; 2006 [in Italian].

[32] prEN 1052-1.1998. Methods of test for masonry—Part1: Determination of compr. strength. Sept. 1998.

[33] prEN 772-1. 1999. Methods of test for masonry units—Part1: Determination of compr. strength. Febr. 1999.

[34] Page AW. The biaxial compressive strength of brick masonry. Proc Instn Civ Engrs 1981;71:893–906.

[35] Ellingwood B, Tallin A. Limit states criteria for masonry construction. J Struct Eng 1985;111:108–22.

[36] Dymiotis C, Gutlederer BM. Allowing for uncertainties in the modelling of masonry compressive strength. Constr Build Mat 2002;16:443–52.

[37] Brencich A, Corradi C, Sterpi E. Experimental approaches to the compressive response of solid clay brickwork. In: 13th IBMaC. 2004.

[38] Brencich A, Morbiducci R. Masonry arches: Historical rules and modern mechanics. Int J Arch Her 2007;1:165–89.